Hybrid Nanocomposite Preparation in a Batch Mixer and a Twin-Screw Extruder

M. OLIVEIRA

Institute for Polymers and Composites/I3N, University of Minho, Campus de Azurém, 4800-058 Guimarães, Portugal

R. NOGUEIRA

Institute of Sanitary Engineering and Waste Management, University of Hannover, D-30167 Hannover, Germany

A. V. MACHADO

Institute for Polymers and Composites/I3N, University of Minho, Campus de Azurém, 4800-058 Guimarães, Portugal

Abstract

Hybrid polymer nanocomposites (HPN) with same composition were prepared in an internal mixer and in an extruder at the same temperature. Polypropylene grafted with maleic anhydride and aluminum isopropoxide were used as organic and inorganic components, respectively. Moreover, the chemical and morphological evolution along the extruder was followed. The HPNs were characterized by several techniques, such as Fourier transform infrared, rheology, X-ray diffraction, gel content, scanning electron microscopy/energy dispersive X-ray spectrometry, and transmission electronic microscopy. Chemical and morphological characterization showed that the sol-gel reaction in the extruder was more extensive; the produced nanocomposite exhibited a higher cross-linking level with smaller and more homogeneous nanoparticles. Along the extruder, the nanoparticles', size decreased as the reaction took place.

KEY WORDS: Crosslinking, Nanoparticles, Reactive processing

Introduction

Polymer systems, since the early to middle 20th century, started to receive considerable attention due to their unique properties, such as easy to produce, lightweight, and often ductile in nature. [1,2] Nevertheless, polymers have lower modulus, strength, and fire

resistance when compared to classic materials, such as metals or ceramics. [1] Therefore, to overcome these disadvantages, the properties can be improved by the addition of inorganic compounds (fibers, whiskers, platelets, or particles) to polymers, [1,3,4] which initiated a new field on polymer research, the polymer nanocomposites. [5] Polymeric inorganic nanocomposites result from nanosize particle inclusions in a polymer matrix, leading to new properties that could not be achieved by the polymer, [6] keeping, at the same time, lightweight and ductile in nature. [1] In fact, a small amount of inorganic fillers, when well dispersed, can significantly improve the material properties, such as gas permeability, thermal stability, flame retardance, mechanical performance, and chemical resistance. [7]

Because nanocomposites result from the combination of at least two phases and the degree of mixing between the two phases has great influence on final nanocomposite properties, the main challenge is to obtain homogeneous nanofiller dispersion in the polymeric matrix. [3,8] Even though a variety of methods to produce polymer nanocomposite have been studied, the most used are melt mixing, in situ polymerization, and in situ sol-gel reactions. [1,6,9,10] According to the literature, in situ sol-gel reactions in the melt is one of the most suitable method to produce dispersed nanoparticles in a polymer matrix without solvent and it can be applied to industrial processes like extrusion. [4,6,11] This approach applies the classic sol-gel method to extrusion; the hydrolysis-condensation reaction of the metal alkoxide precursor can directly occur in the polymer melt. [6,12] The extruder and internal mixer act as a continuous or batch chemical reactor, respectively.

It is known that reactive extrusion is a complex process with many variables that can change during the process. Residence time, pressure, temperature, mixing, and diffusion are parameters that govern the material's final properties. [11] Therefore, sometimes for research work, an internal mixer, with fewer variables to consider, is used to develop materials. Nevertheless, at the same time, internal mixers are used to simulate the extrusion process. Thus, the main objective of this work is to compare the preparation of hybrid nanocomposites in an internal batch mixer and a twin-screw extruder. Moreover, the chemical reaction evolution and nanoparticle dispersion along the extruder were also assessed. Nanocomposites with the same composition were prepared in an internal mixer and a twin-screw extruder at the same temperature. The materials were characterized by several techniques, such as Fourier transform infrared (FT-IR), rheology, X-ray diffraction (XRD), gel content, scanning electron microscopy(SEM)/energy dispersive X-ray spectrometry (EDS), and transmission electronic microscopy (TEM).

Materials and Methods

MATERIALS AND REAGENTS

Polypropylene modified with maleic anhydride (PP-g-MA; Polybond 3200) with a melting temperature around 160°C and a MA content of 1wt%, was supplied by Crompton (Middlebury, CT). Aluminum isopropoxide ($Al(Pr-i-O)_3$) was used as received and was supplied by Sigma Aldrich (Sintra, Portugal).

NANOCOMPOSITE PREPARATION

Internal Mixer

PP containing aluminum nanoparticles was prepared in the melt, in a Haake batch mixer (Rheocord 90; volume 60 mL), equipped with two rotors

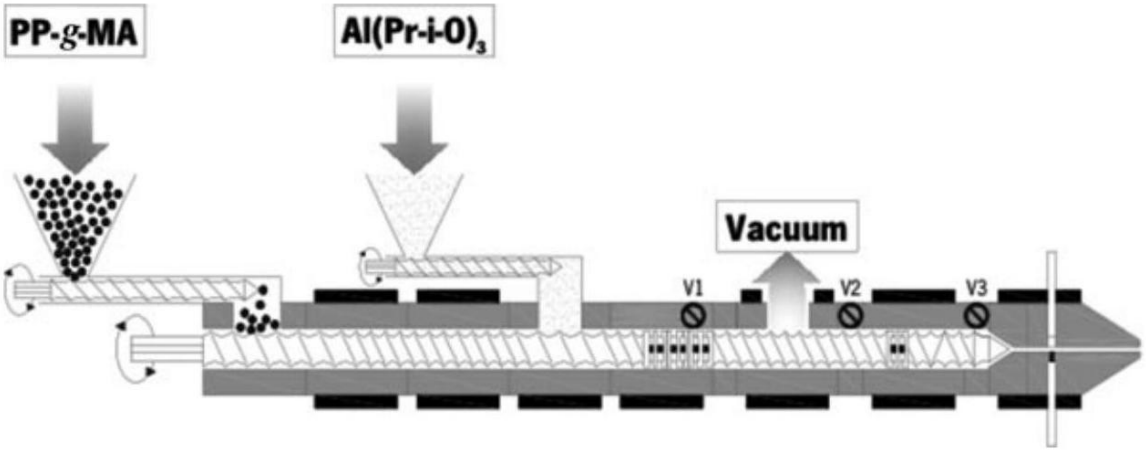

FIGURE 1. Extruder layout.

running in a counterrotating way. The rotor speed was 50 rpm , and the set temperature was 180°C. The following procedure was adopted to prepare the nanocomposites: First pellets of PP-g-MA were introduced into the hot mixer; after melting, the aluminum precursor was added (15 and 25wt%). The total sample was removed after 10 min of mixing. The hybrid nanocomposite (HPN) synthesized in the internal mixer was called HPN-int.

Extruder

A modular corotating twin-screw extruder, Leistritz LSM 30.34, was used (Fig. 1). As in the internal mixer, 15wt% of aluminum precursor was added using a side feeder to PP- *g*-MA after melting. The barrel set temperature was 180°C, the screw speed 200 rpm , and the throughput 3.8 kg/h. The average residence time at the various sampling locations along the extruder, under the selected operating conditions, estimated using a tracer impulse technique, was 65, 105, 139, and 160 s for V1, V2, V3, and extrudate, respectively.

The molten polymer samples were collected along the screw axis and from the extrudate, and then quenched in liquid nitrogen to avoid further reaction (about 3 g of sample in 300 mL liquid nitrogen). [13] The HPN synthesized in the extruder was called HPN-ext.

CHARACTERIZATION

FT-IR

Infrared spectra of all HPNs were recorded in transmission mode between 400 and 4000 cm^{-1} using a Perkin-Elmer 1610 spectrometer, with 32 scans

and a resolution of 4 cm^{-1}. Thin films were previously prepared by compression molding in a hot press at 180°C and analyzed directly using a solid film support.

X-Ray Diffraction

XRD spectra of the samples were obtained at room temperature using a Bruker D8 Discover Xray equipment with a Ni-filter. The applied current and accelerating voltage were 40 mA and 40 kV , respectively.

Rheological Properties

The rheological behavior of the initial polymers and prepared HPNs was determined by oscillatory rheological measurements carried out in a Paar Physica MCR300 rheometer at 90°C. The gap and diameter of the plates was 1 and 25 mm , respectively. Nitrogen atmosphere was used to prevent thermooxidative degradation. A frequency sweep from 0.1 to 100 Hz under constant strain in the linear viscoelastic region was performed for each sample.

Gel Content and Cross-Linking Density

Around 150 mg of samples were used to determine the gel content. The materials, previously weighted, were placed in a 125-mesh stainless steel basket and immersed in hot xylene at 140°C for 30 h . The final weight was determined after drying the samples in a vacuum oven at 105°C for the night. The gel content was calculated as the weight of nonextractable material divided by the total weight of the original sample and is expressed as a percentage.

The cross-linking density was assessed from the volume swelling degree determined at equilibrium, as described by Oliveira et al. [14]

Morphological Characterization

SEM analysis was performed using a Leica Cambridge S360 microscope. The samples were previously fractured in liquid nitrogen and coated with a gold thin film. X-ray microanalysis mapping was performed on $300\mu\,m^2$ in the same place where SEM micrographs were recorded, with EDS from Link eXL II from Oxford Instruments attached to the SEM.

TEM micrographs were taken from samples of 70-nm thickness cut using a diamond knife, in a Leica ultramicrotome at −40°C. The cut sections were transferred onto copper grids and then analyzed without staining in a Philips CM120, TEM.

Results

COMPARISON BETWEEN INTERNAL MIXER AND EXTRUDER PREPARATION

The FT-IR spectra of PP-g-MA, HPN-int, and HPN-ext are shown in Fig. 2a. Nanocomposites prepared in the internal mixer and in the extruder present two new bands between 1000-400 and 35003000 cm^{-1}, corresponding to $Al-O$ and OH stretching modes, respectively. The OH band, with respective bending mode band at 1627 cm^{-1}, confirms that the precursor has undergone hydrolysis. The presence of the $Al-O$ band indicates that sol-gel reaction was successfully carried out.

Comparing the spectra of HPN-int and HPNext, it is clear that the OH band is smaller for the latter even though with less reaction time. This can be associated with higher reaction extension in the extruder and highly efficient removal of the reaction byproduct (2-propanol, C_3H_7OH) [9] as a result of devolatilization applied on the extruder barrel (Fig. 1).

A more detailed inspection of the region 850-400 evidences more differences between the two prepared materials (Fig. 2b). In the HPN structure, aluminum oxide can exist in two different coordination states, tetrahedral and octahedral. [15,16] A broad band extending from 500 to 750 cm^{-1} confirms the presence of tetrahedral $Al-O$ coordination and bands at 500 and 640 cm^{-1} are assigned to octahedral coordination. Although these two bands can be clearly seen for HPN-ext indicating octahedral coordination, only a broad band is presented in HPN-int, suggesting tetrahedral Al-O coordination. This difference is directly related to the extension of the solgel reaction and, consequently, with cross-linking density. Extensive sol-gel reactions result in higher levels of cross-linking density and different distribution of the inorganic domains.

The XRD spectra of PP-g-MA, HPN-int, and HPN-ext are shown in Fig. 3. The comparison of HPN-int and HPN-ext with PP-*g*-MA reveals new peaks at $19.8°, 20.9°, 23.9°$, and $44.23°$, which are in agreement with the study of Oliveira et al. [9] Moreover, the results reveal that the two methods used to prepare the nanocomposites do not affect the final microstructure of obtained nanocomposites. Then, the new peaks might be due to the presence of aluminum oxide hydroxide (AlOOH) and aluminum hydroxide ($Al(OH)_3$), as it was observed in the FTIR spectra. Nevertheless, the total number of peaks characteristic of either AlOOH or $Al(OH)_3$ is not present in the spectra, which makes difficult to conclude whether these two species are really present.

As shown by FT-IR, Al(Pr-i-O) $_3$ reacts with PP-*g*-MA to form covalent bonds with the polymer backbone. Because the precursor has three reactive groups, it can create maximum three covalent bonds with PP. Therefore, depending on the reaction extension, a polymer with different cross-linking degrees can be produced. Rheological measurements can provide additional information on cross-linking. The rheological behavior of HPN-int and HPN-ext with the same and different compositions depicted in Fig. 4 shows a significant difference in viscosity and storage modulus between HPN-int and HPNext. Moreover, it is possible to observe that HPN-ext has the same viscosity as the nanocomposite produced in the internal mixer with 25wt% of precursor. This significant improvement in viscosity of the HPN-ext can be associated with the mixing efficiency in the extruder, which resulted in a more efficient sol-gel reaction and

consequently more crosslinking. The storage modulus also increases and has the same trend for the same amount of the precursor. This change can be associated with the transition from liquid-like to solid-like behavior, where storage modulus is almost constant in all frequency ranges, as it can be observed for HPN-ext. This type of behavior is characteristic of a material with a high cross-linking level.

The gel content and cross-linking density, listed in Table I, confirm the difference detected for viscosity and storage modulus; HPN-ext has the similar gel content and cross-linking level to HPN-int

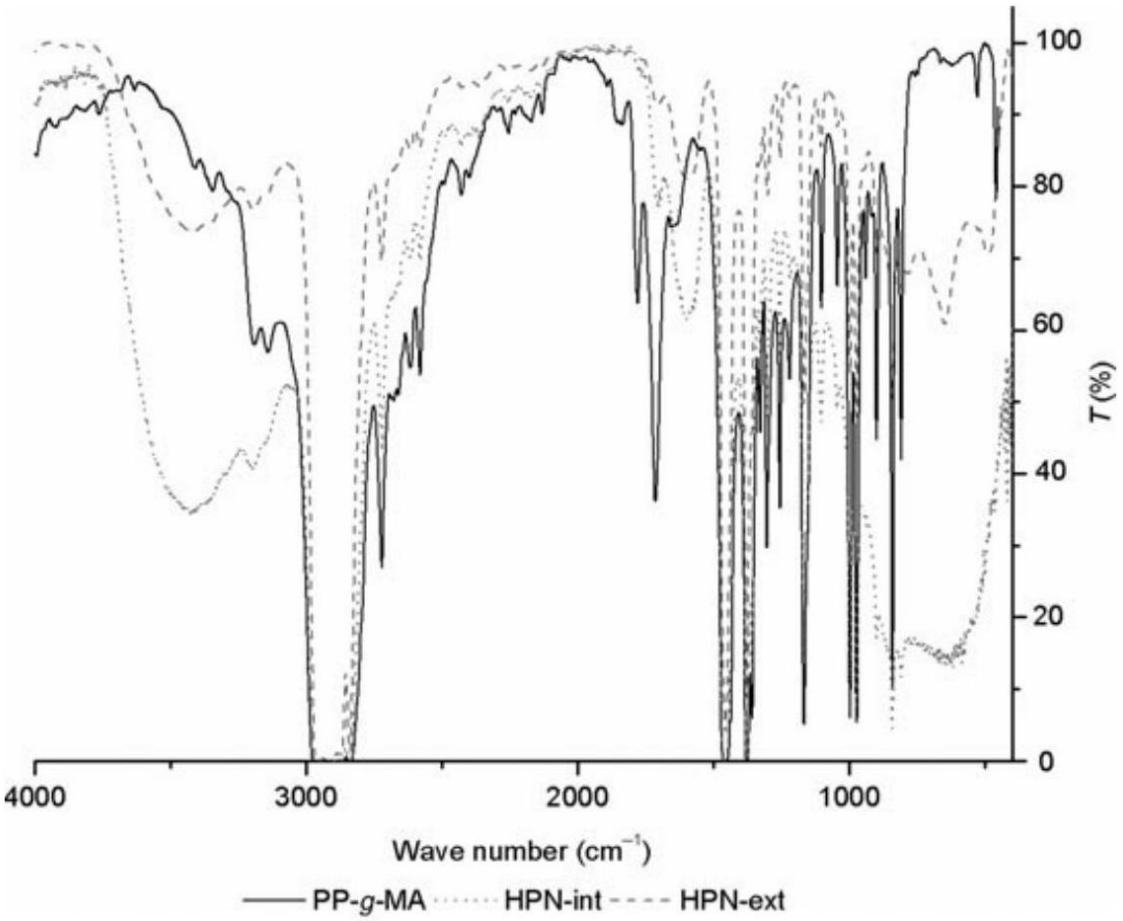
100
80
60
40
20
0
T (%)
4000
3000
2000
1000
Wave number (cm^{-1})
PP-g-MA
HPN-int
HPN-ext

(a)

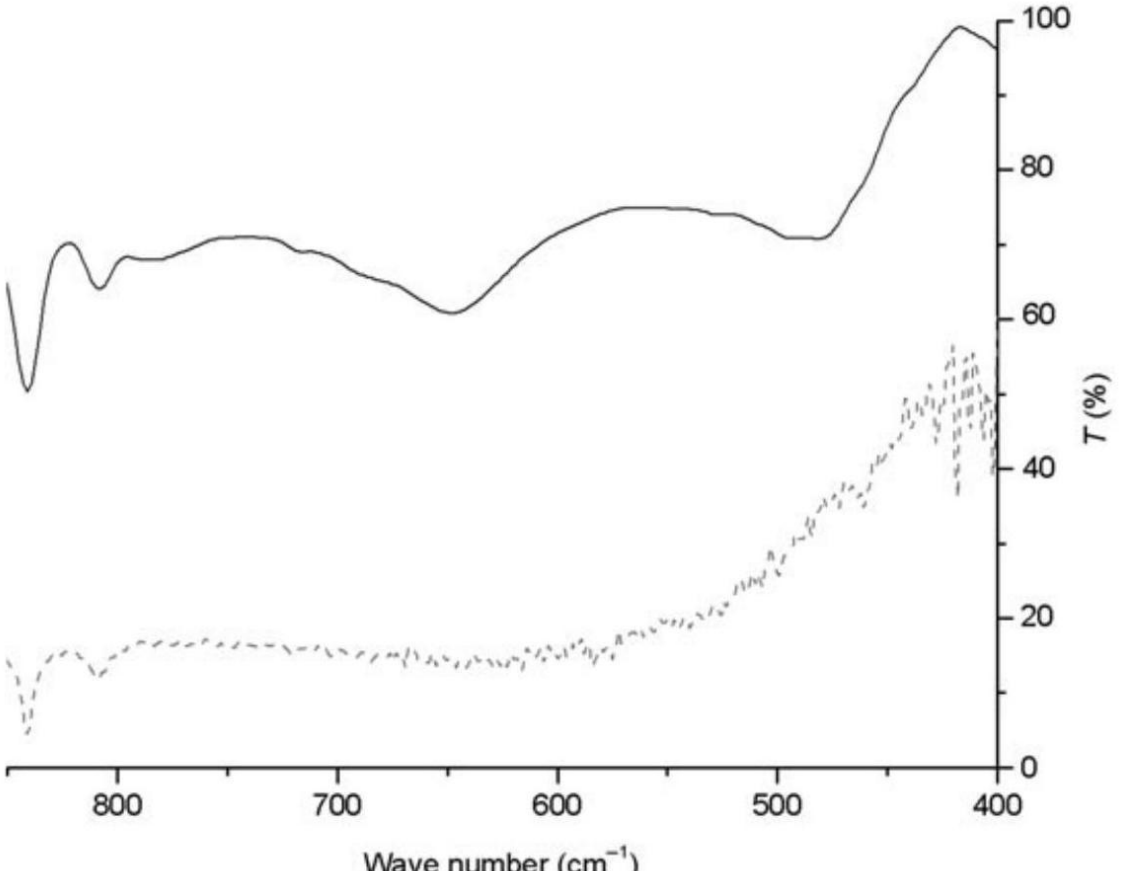
100
80
60
40
20
0
T (%)
800
700
600
500
400
Wave number (cm^{-1})

FIGURE 2. (a) FT-IR spectra of PP-g-MA, HPN-int, and HPN-ext. (b) FT-IR spectra of PP-g-MA, HPN-int, and HPN-ext between 500 and 850 cm^{-1}.

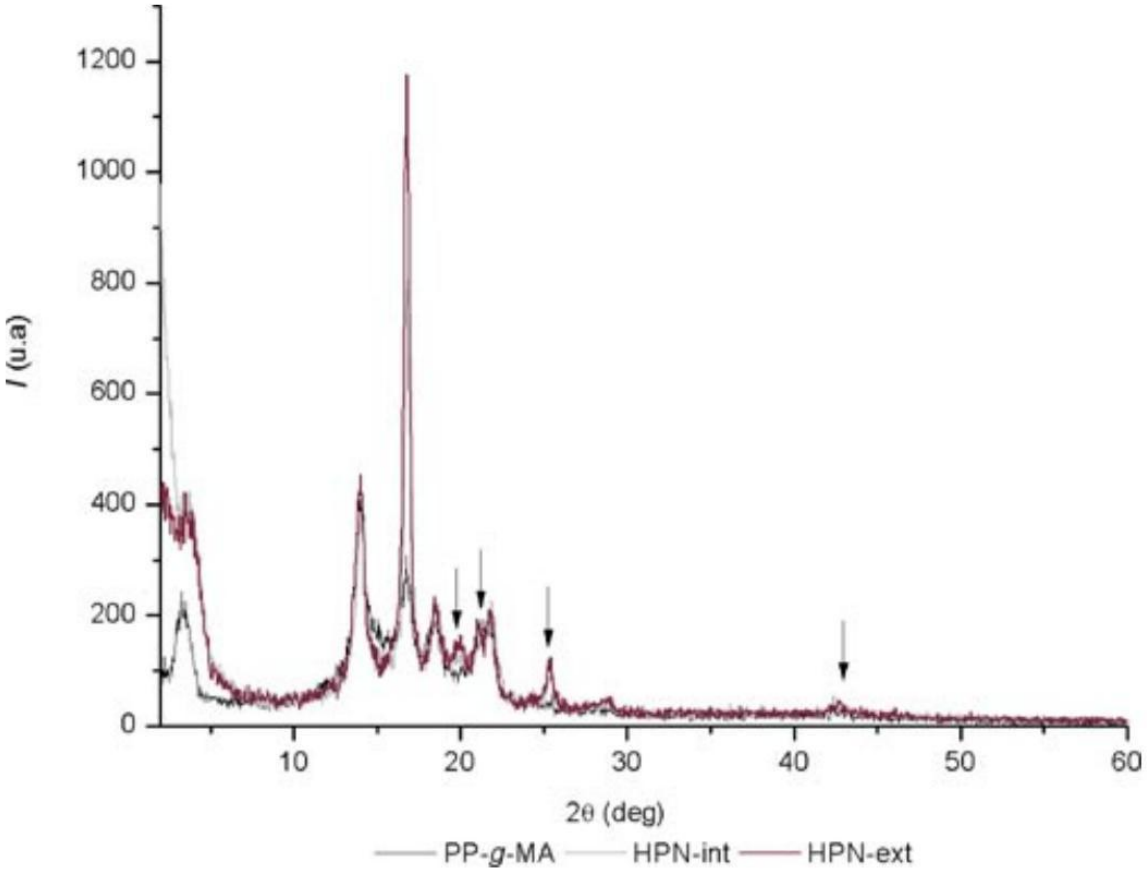

FIGURE 3. XRD pattern for PP-g-MA, HPN-int, and HPN-ext.

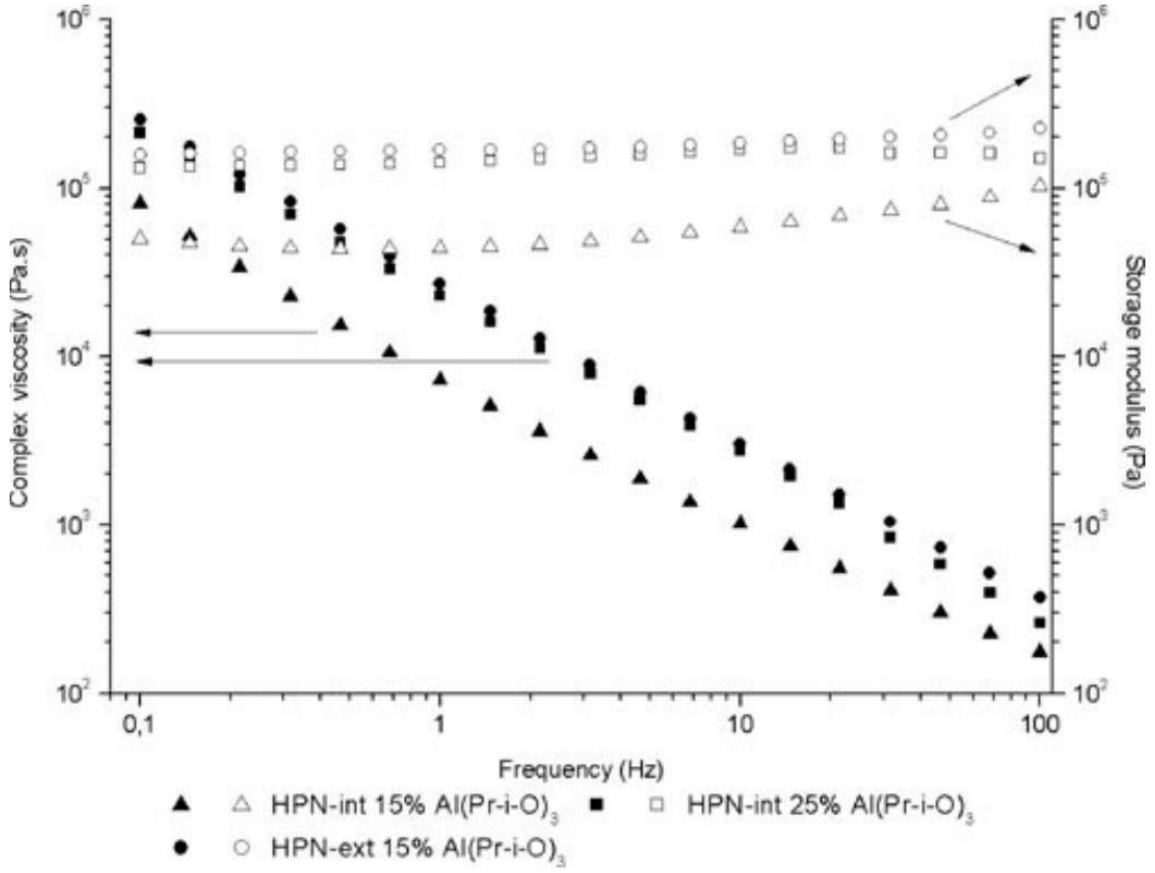

FIGURE 4. Rheological behavior of HPNs.

TABLE I
Gel-Content and Cross-Linking Values for Nanocomposites Prepared in Internal Mixer and Extruder

Samples	Gel Content (%)	Cross-Linking Density (mol/mL)
HPN-int 15wt% precursor	48.7 ± 3.2	$77.7 \times 10^{-6} \pm 5.78 \times 10^{-6}$
HPN-int 25 wt% precursor	71.0 ± 1.6	$105 \times 10^{-6} \pm 2.08 \times 10^{-6}$
HPN-ext 15wt% precursor	69.6 ± 1.9	$118 \times 10^{-6} \pm 9.99 \times 10^{-6}$

Unmarked set by manueloliveira.

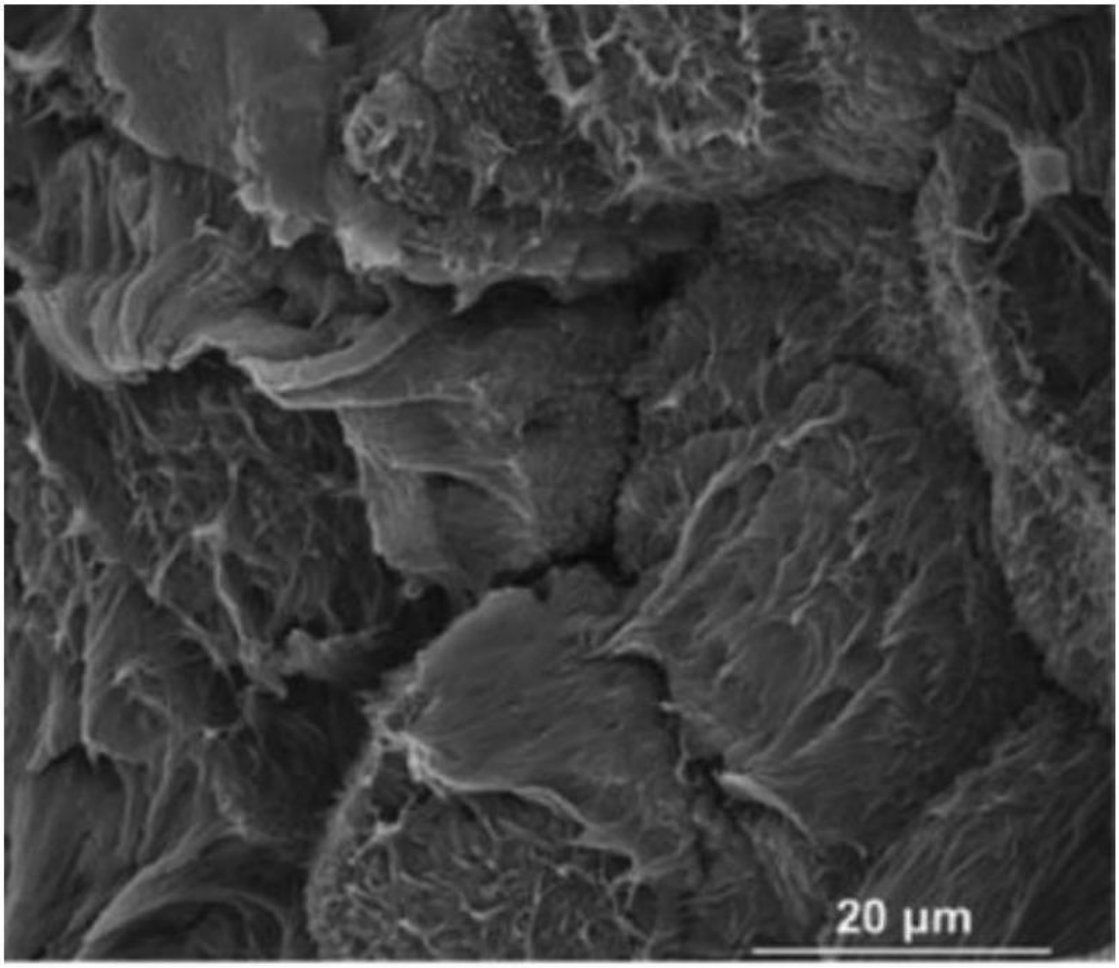

(a)

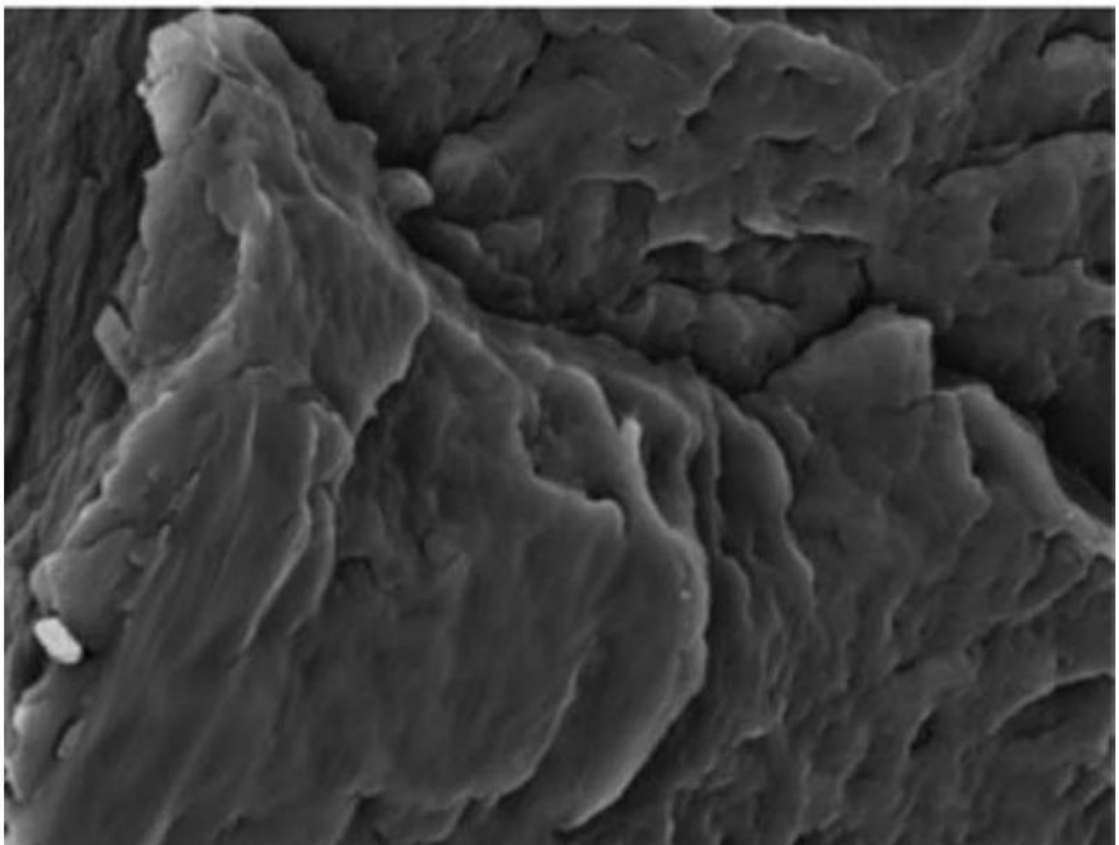

FIGURE 5. SEM micrographs of (a) HPN-int and (b) HPN-ext. produced with 25*wt*% of the precursor. However, the gel content obtained with the same composition is different, 48.7% and 69.6% for HPN-int and HPNext, respectively. These results corroborate the FT-IR and rheological measurements that indicate that the sol-gel reaction was more extensive in the extruder.

The SEM micrographs, in backscattered electrons mode, of HPNs fracture surfaces, are present in Fig. 5. While HPN-int exhibits a heterogeneous surface (Fig. 5a), the HPN-ext micrograph (Fig. 5b) shows a homogeneous and smooth surface, more cohesive and regular than HPN-int. Owing to the small particle size. it was not possible to detect any inor-

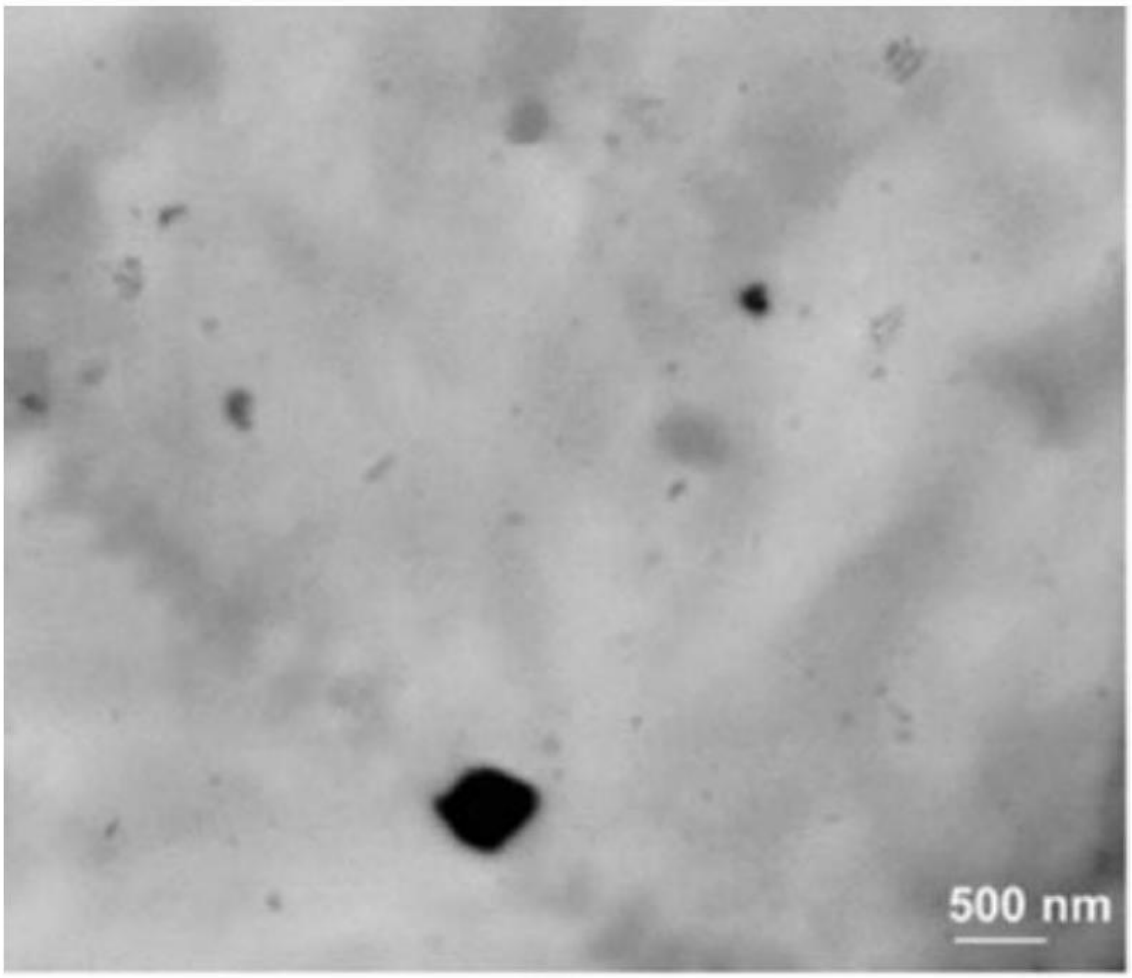

(a)

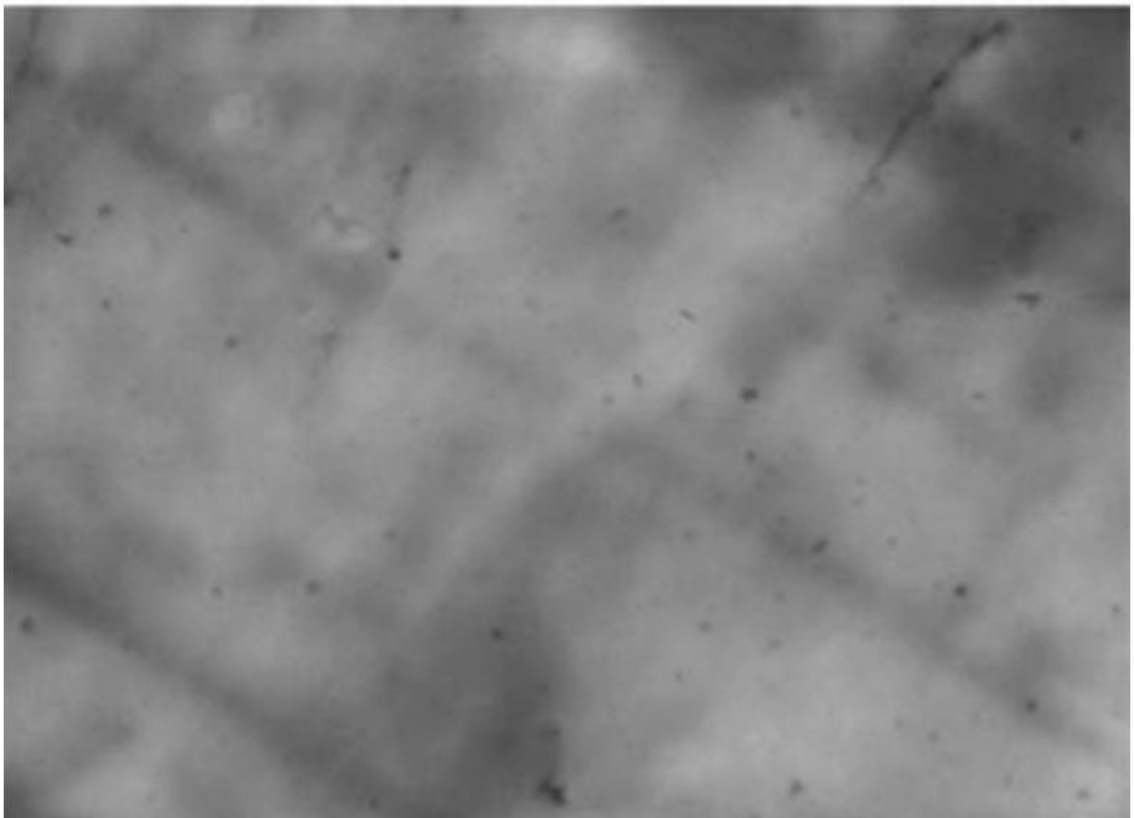

FIGURE 6. TEM micrographs of (a) HPN-int and (b) HPN-ext. ganic particles. Therefore, TEM analysis was accomplished to assess the size and dispersion of nanoparticles achieved by the two preparation methods.

TEM micrographs depicted in Fig. 6 clearly show that HPN-ext (Fig. 6b) has a better particle dispersion with a smaller particle size, around 85 nm . HPN-int (Fig. 6a) presents a very poor dispersion and bigger particles, around 155 nm . Because the reaction was more extensive in the extruder, which resulted in a higher cross-linking level, a better dispersion and smaller nanoparticle would be anticipated for HPN-ext.

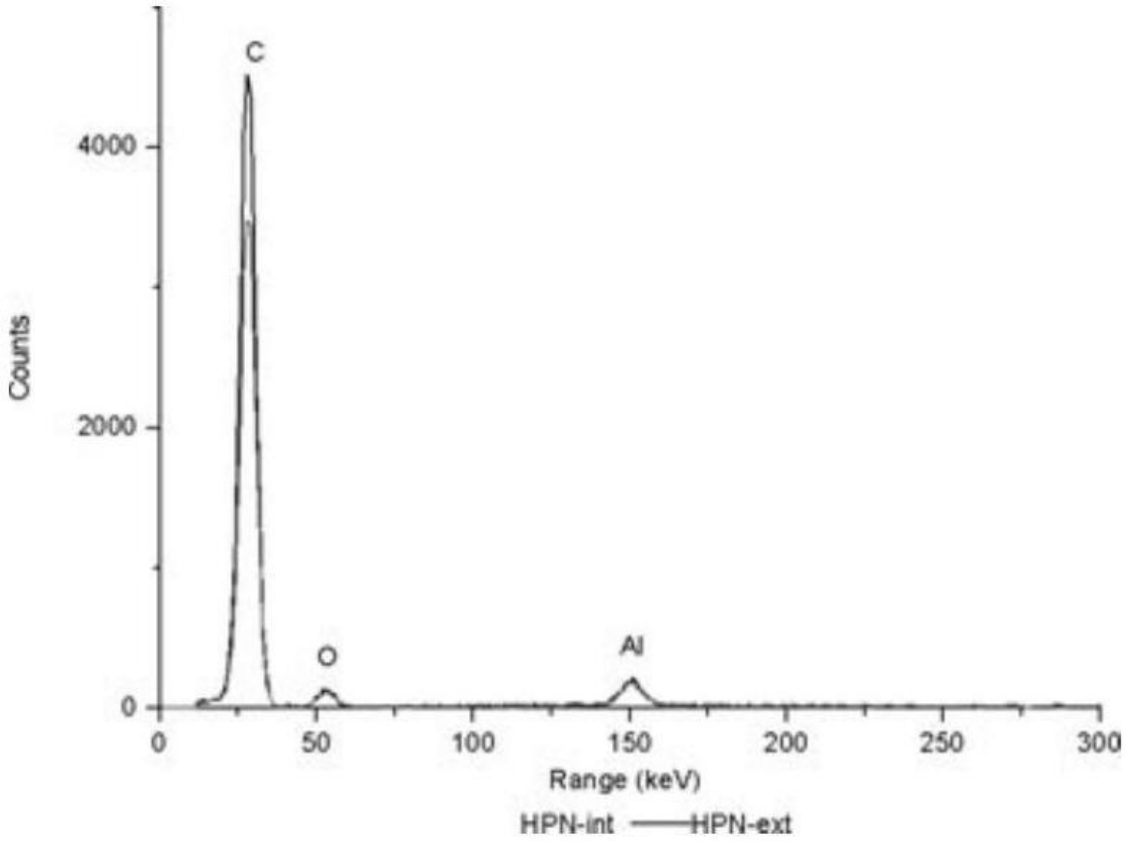

FIGURE 7. EDS spectrum of HPN surfaces.

The EDS analysis (Fig. 7) was performed to confirm that the nanoparticles of both HPNs contained aluminum. A similar value of aluminum content, for both nanocomposites, was obtained from quantification of spectra peaks.

EVOLUTION ALONG THE EXTRUDER

To follow the reaction evolution and morphology along the extruder during HPN-ext preparation, the samples collected at three different locations along

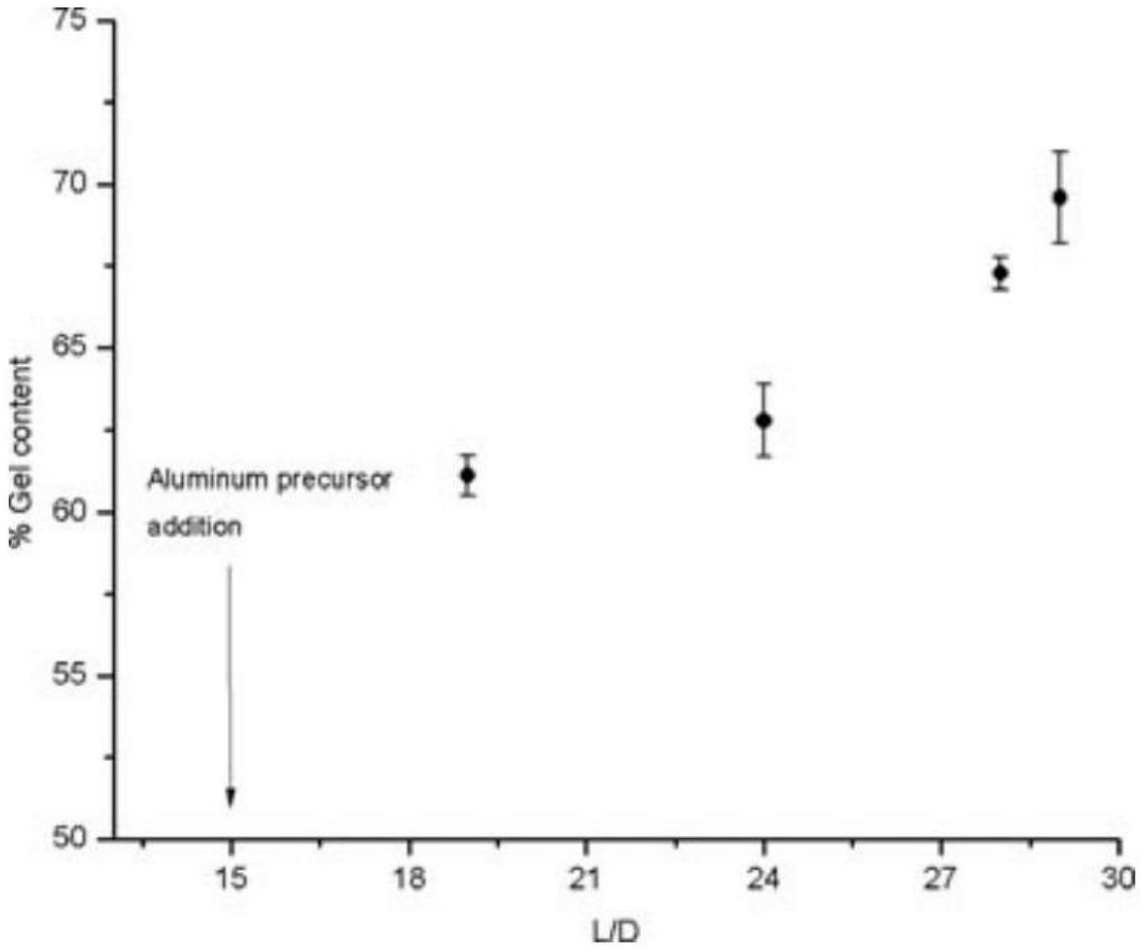

FIGURE 9. Gel content evolution of HPN-ext along the extruder screw. the screw barrel (V1, V2, V3) and extrudate (Fig. 1) were characterized by FT-IR, gel content, and TEM. Figure 8 shows the FT-IR spectra of the samples collected along the extruder. The spectrum of the sample collected at V1 indicates that the reaction started very quickly, immediately after the addition of the precursor. However, along the extruder, differences can be noticed at 3500-3000 cm $^{-1}$ and 1000-400 cm $^{-1}$

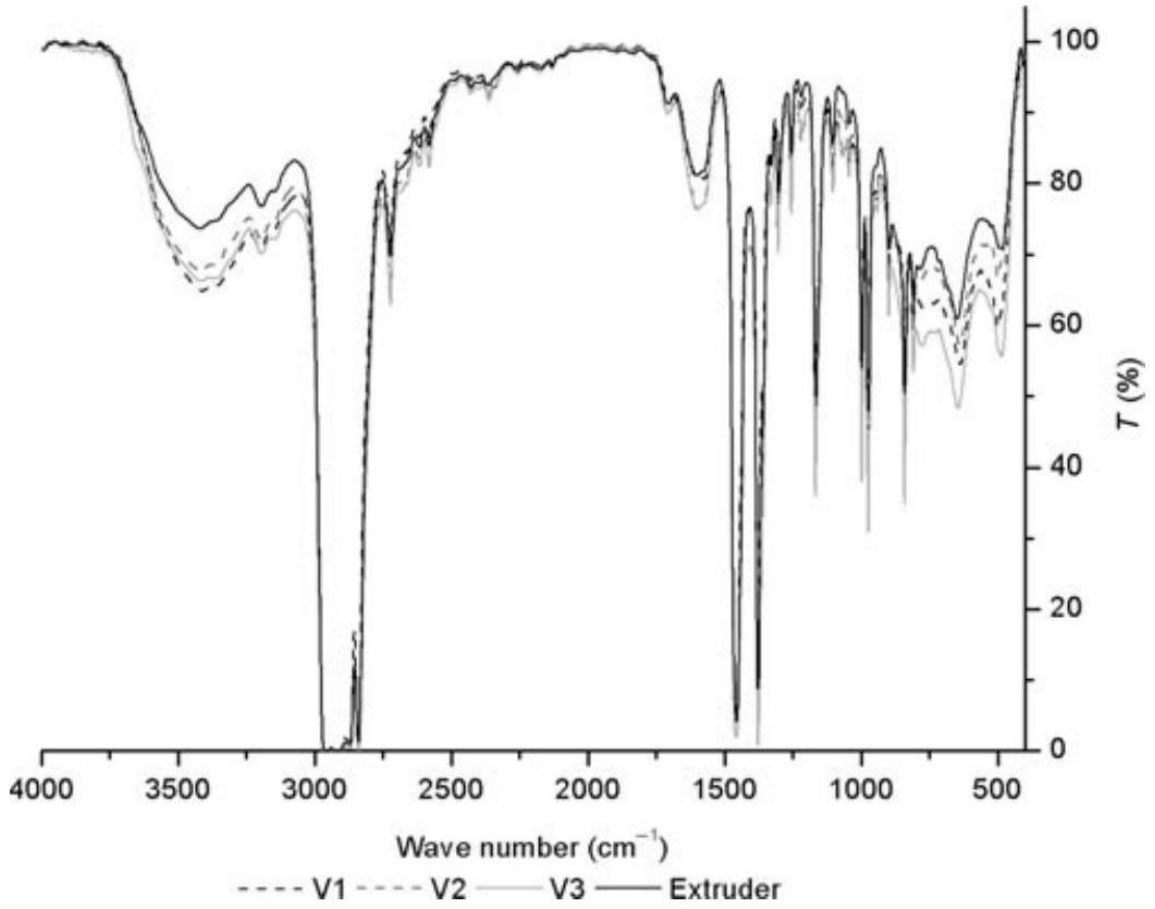

FIGURE 8. FT-IR spectra evolution of HPN-ext along the extruder screw.

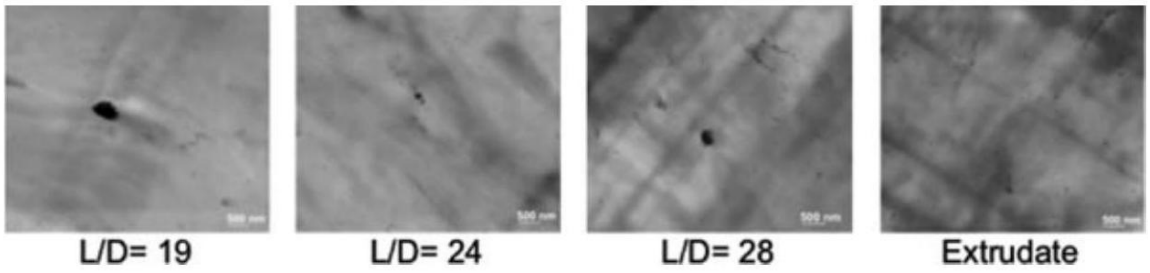

FIGURE 10. TEM micrographs of HPN-ext along the extruder and extrudate. corresponding to OH and $Al-0$ stretching modes, respectively. The decrease in the intensity of the band between 3500 and 3000 cm^{-1} along the extruder reveals that the reaction is still going on until the extrudate. These results are in line with the gel content determination, at the first sampling location the gel content was already around 60%, it increases along the barrel reaching a value of 70% for the extrudate (Fig. 9).

TEM micrographs of the collected samples provide information about the particles', dispersion evolution along the extruder (Fig. 10). At location L/D 19, a heterogeneous dispersion can be noticed with an average particle size of 150 nm . The particle size is 130 and 98 nm for L/D 24 and 28, respectively. A homogeneous dispersion with small particles

(85 nm) was achieved for the extrudate. Taking into account the FT-IR, gel content results, and TEM micrographs, the particle size decreases as the reaction takes place.

Conclusions

Hybrid polymer nanocomposites with the same composition were prepared in an internal mixer and in a twin-screw extruder at the same temperature.

Both FT-IR and rheological measurements showed that the sol-gel reaction was more extensive in the extruder. The nanocomposite prepared exhibited a more cross-linked structure. TEM micrographs evidenced that this nanocomposite presented smaller and well-dispersed nanoparticles.

Both chemical reaction extent and morphology evolution vary along the extruder. The particle size decreased as the chemical conversion increased.

References

1. Jordan, J.; Jacob, K.; Tannenbaum, R.; Sharaf M.; Jasiuk, I. Mater Sci Eng A 2005, 393, 1.
2. Schultz, J. Polymer Materials Science; Prentice-Hall: Englewood Cliffs, NJ, 1974.
3. Ishida, H.; Campbell, S.; Blackwell, J. Chem Mater 2000, 12, 1260.
4. Di, Y.; Iannace, S.; Maio, E.; Nicolais, L. J Polym Sci, Part B: Polym Phys 2003, 41, 670.
5. Krishnamoorti, R.; Vaia, R. Polymer Nanocomposites: Synthesis, Characterization and Modeling; American Chemical Society: Washington, DC, 2002.
6. Dou, D.; Zhu, X.; Peter, K.; Demco, D.; Möller, M.; Melian, C. J Sol-Gel Sci Technol 2008, 48, 51.
7. Bahloul, W.; Bounor-legaré, V.; David, L.; Cassagnau, P. J Polym Sci, Part B: Polym Phys 2010, 48, 1213.
8. Cong, H.; Radosz, M.; Towler, B.; Shen, Y. Sep Purif Technol 2008, 55, 281.
9. Oliveira, M.; Nogueira, R.; Machado, A.V. React Funct Polym 2012, 72, 703.
10. Rong, M.; Zhang, M.; Zheng, Y.; Zeng, H.; Walter, R.; Friedrich, K. Polymer 2001, 42, 167.
11. Bahloul, W.; Oddes, O.; Bounor-legaré, V.; Mélis, F.; Cassagnau, P.; Vergnes, B. AIChE J 2011, 57, 2174.
12. Wanga, Y.; Chena, F.; Lib, Y.; Wu, K. Composites, Part B 2004, 35, 111.
13. Machado, A. V.; Covas, J. A.; Duin, M. J Appl Polym Sci 1999, 71, 135.
14. Oliveira, M.; Nogueira, R.; Machado, A. V. Polym Intern. Under review.
15. Joe, I. H.; Vasudevan, A. K.; Aruldhas, G.; Damodaran, A. D.; Warrier, K. G. K. J Solid State Chem 1997, 131, 181.

16. Wengrovius, J. H.; Garbauskas, M. F.; Williams, E. A.; Going, R. C.; Donahue, P. E.; Smith, J. F. J Am Chem Soc 1986, 108, 982.